Title

Enterococcus faecalis α1-2-mannosidase (EfMan-I): an efficient catalyst for glycoprotein N-glycan modification.

Journal

FEBS letters, 594(3)

ISSN

0014-5793

Authors

Li, Yanhong
Li, Riyao
Yu, Hai
et al.

Publication Date

2020-02-01

DOI

10.1002/1873-3468.13618

Peer reviewed

FEBS Letters

FEBS PRESS science publishing by scientists

Enterococcus faecalis α1–2-mannosidase (EfMan-I): an efficient catalyst for glycoprotein N-glycan modification

Yanhong Li[1], Riyao Li[1], Hai Yu[1], Xue Sheng[1], Jing Wang[1,2], Andrew J. Fisher[1,3] and Xi Chen[1]

1 Department of Chemistry, University of California, Davis, CA, USA
2 Key Laboratory of Experimental Marine Biology, Institute of Oceanology, Chinese Academy of Sciences, Qingdao, China
3 Department of Molecular and Cellular Biology, University of California, Davis, CA, USA

Correspondence
X. Chen, Department of Chemistry, University of California, Davis, California 95616, USA
Tel: 530-754-6037
E-mail: xiichen@ucdavis.edu

Yanhong Li and Riyao Li contributed equally to this work

(Received 6 July 2019, revised 18 September 2019, accepted 19 September 2019)

doi:10.1002/1873-3468.13618

Edited by Judit Ovádi

While multiple α 1–2-mannosidases are necessary for glycoprotein N-glycan maturation in vertebrates, a single bacterial α1–2-mannosidase can be sufficient to cleave all α1–2-linked mannose residues in host glycoprotein N-glycans. We report here the characterization and crystal structure of a new α1–2-mannosidase (EfMan-I) from *Enterococcus faecalis*, a Gram-positive opportunistic human pathogen. EfMan-I catalyzes the cleavage of α1–2-mannose from not only oligomannoses but also high-mannose-type N-glycans on glycoproteins. Its 2.15 Å resolution crystal structure reveals a two-domain enzyme fold similar to other CAZy GH92 mannosidases. An unexpected potassium ion was observed bridging two domains near the active site. These findings support EfMan-I as an effective catalyst for *in vitro* N-glycan modification of glycoproteins with high-mannose-type N-glycans.

Keywords: alpha-mannosidase; crystal structure; glycoprotein modification; mannosidase; N-glycan enzymatic modification

N-Linked glycan modification is an important post-translational modification (PTM) of proteins that affects their conformation, solubility, stability, immunogenicity, and recognition by other molecules [1,2]. In fact, many therapeutic proteins are N-glycosylated glycoproteins and proper glycosylation is important for their pharmacokinetics, cellular distributions, and biological activities [3–5]. Glycan engineering of therapeutic glycoproteins has shown to improve their functions [6–8]. Among various methods [9–11] including glycoengineering of host biosynthetic pathways [12–14], chemoselective ligation of tagged proteins and glycans [10,11], total chemical synthesis by native chemical ligation [15], *in vitro* chemoenzymatic glycosylation remodeling [16], and *in vitro* enzymatic glycosylation of glycoproteins [8], the latter is an attractive strategy to produce glycan-defined glycoproteins [8].

In eukaryotes, N-glycosylation is a part of a glycoprotein quality control process in the endoplasmic reticulum (ER). Eukaryotic N-glycans usually belong to one of the three types of structures including oligomannose, complex, and hybrid. These structures share a common tri-mannose core Man α1–3(Manα1–6) Manβ1–4GlcNAcβ1–4GlcNAcβ1–(Asn-X-Ser/Thr) but differ on the extension at the non-reducing end [17], with or without an additional core fucose [18], and the linkage of the core fucose [19]. Oligomannose-type (or high-mannose type) N-glycans can be considered as precursors for the biosynthesis of complex and hybrid-type N-glycans in glycoproteins. Early steps of such conversion involve trimming high-mannose N-glycans by α1–2-mannosidase-catalyzed reactions. In human, multiple α1–2-mannosidases, including ER α1–2-mannosidase I (ERManI) and three Golgi

Abbreviations
2-AB, 2-aminobenzamide; EfMan-I, efficient α1–2-mannosidase; EfMan-I, *Enterococcus faecalis* α1–2-mannosidase; ER, endoplasmic reticulum; HAIs, health care-associated infections; HPLC, high-performance liquid chromatography; IPTG, isopropyl-1-thio-D-galactopyranoside; MS, mass spectrometry; PTM, post-translational modification; SSRL, Stanford Synchrotron Radiation Lightsource.

F E B 2 Journal Code 13618 Manuscript No. WILEY Dispatch: 30.9.19 No. of pages: 13 CE: Ishwarya R PE: Bhagyalakshmi

α1–2-mannosidases (GM1A, GM1B, and GMIC), are responsible for removing four α1–2-linked mannose from high-mannose-type N-glycan $Man_9GlcNAc_2$ to form $Man_5GlcNAc_2$ [20]. In comparison, α1–2-mannosidases capable of catalyzing the cleavage of all four α1–2-mannose residues in high-mannose type N-glycan $Man_9GlcNAc_2$ have been identified in a limited number of bacteria such as *Bacteroides thetaiotaomicron* VPI-5482 (Bt3990 and Bt2199) [21], *Streptococcus pneumoniae* (SpGH92) [22], and *Cellulosimicrobium cellulans* [23]. An exo-1,2-α-D-mannanase purified from *Bacillus* sp. M-90 has also been shown to catalyze the cleavage of all α1–2-linked mannose residues in $Man_9GlcNAc_2$ to form $Man_5GlcNAc_2$ [24]. All known exo-α1–2-mannosidases are mainly classified into three glycoside hydrolase (GH) families in the Carbohydrate Active Enzyme (CAZy) database (http://www.cazy.org) [25–27] including GH38, GH47, and GH92. While characterized mammalian ER and Golgi α1–2-mannosidases are in the CAZy GH47 family [20], most bacterial α1–2-mannosidases characterized so far are in the GH92 family, and lysosomal α-mannosidases are in the GH38 family.

Bacterial α1–2-mannosidases are attractive enzymes for *in vitro* enzymatic glycan modification of the high-mannose-type N-glycans in natural and recombinant glycoproteins to hybrid or complex-type N-glycans. They are also appealing targets for better understanding how host glycoprotein glycans can be utilized by commensals and pathogenic bacteria to shape microbiota community [28]. By sequence alignment and literature survey, we identified EF2217 from *Enterococcus faecalis* V583 [29], a member in the CAZy GH92 family, as a promising candidate for a novel and highly active bacterial α1–2-mannosidase. *E. faecalis* is a Gram-positive commensal bacterium and an opportunistic pathogen that can cause health care-associated infections (HAIs) including urinary tract infections, bacteremia, and infective endocarditis [30]. It was the first clinical vancomycin-resistant enterococcal isolate reported in the USA [31], and the full genomic DNA of strain V583 was reported in 2003 [29]. More importantly, the bacterium was shown to be able to use high-mannose-type N-glycans efficiently but not sialylated N-linked glycans for growth [32]. Two endo-β-N-acetylglucosaminidases from *E. faecalis* V583 (EF0114 and EF2683) were isolated and found to be able to cleave high-mannose N-glycan from glycoprotein to form a single N-linked *N*-acetylglucosamine (GlcNAc) residue [32–34]. Activities of exo-mannosidases in producing free mannose residues from the N-glycans released from glycoproteins were also observed [32] but not characterized. We describe here that EF2217 is an efficient α1–2-mannosidase (EfMan-I) catalyzing the cleavage of α1–2-linked mannose residues from not only synthetic mannosides and high-mannose N-glycans released from glycoproteins, but also high-mannose N-glycans on glycoproteins. The enzyme is thus an effective catalyst and a very useful tool for *in vitro* enzymatic modification of glycoproteins with high-mannose-type N-glycans. The crystal structure reveals that it shares high similarity with other bacterial GH92 α-mannosidases, with an N-terminal β-sandwich domain and a C-terminal α-helical domain. The active site lies in a cleft between the two domains and contains a catalytic calcium ion. An unexpected potassium ion was also observed bridging the two domains near the active site that may help position the two domains.

Materials and methods

Bacterial strains, plasmids, and materials

Escherichia coli electrocompetent DH5α and chemically competent BL21 (DE3) cells were purchased from Invitrogen (Carlsbad, CA, USA). Genomic DNA of *E. faecalis* V583 (ATCC#700802D-5) was from American Type Culture Collection (ATCC, Manassas, VA, USA). Vector plasmid pET22b(+) was from Novagen (EMD Biosciences Inc. Madison, WI, USA). Restriction enzymes NdeI and XhoI were purchased from New England Biolabs, Inc. (Beverly, MA, USA). Nickel-nitrilotriacetic acid agarose (Ni^{2+}-NTA agarose) was from Qiagen (Valencia, CA, USA). GeneJET Plasmid Miniprep kit and GeneJET PCR Purification kit were from Thermo Scientific (San Diego, CA, USA). Herculase-enhanced DNA polymerase was from Stratagene (La Jolla, CA, USA). T4 DNA ligase and 1 kb DNA ladder were from Promega (Madison, WI, USA). *para*-Nitrophenyl-α-D-mannopyranoside (Manα*p*NP) was from Chem-Impex Int'L Inc. (Wood Dale, IL, USA). α2-Mannobiose, α3-mannobiose, and 3α,6α -mannopentaose (Man_5) were from Santa Cruz Biotechnology (Dallas, TX, USA). α6-Mannobiose, hexokinase from *S. cerevisiae*, phosphoglucose isomerase from baker's yeast, and glucose-6-phosphate dehydrogenase from *L. mesenteroides* were from Sigma-Aldrich (Saint Louis, MO, USA). 1,3-α-1,6-α-D-Mannotriose (Man_3) was purchased from Carbosynth Limited (San Diego, CA, USA). *E. coli* phosphomannose isomerase was from Megazyme (Chicago, IL, USA).

Cloning of EfMan-I

Efficient α1–2-mannosidase was cloned as a C-His_6-tagged fusion protein in pET22b(+) vector using genomic DNA of *E. faecalis* V583 (ATCC#700802D-5) as the template for PCRs. The primers used were as follows: forward primer

5′-GATC*CATATG*AATATTCAAGCGATTGATACGCG-3′ (NdeI restriction site is italicized) and reverse primer 5′-ACGC*CTCGAG* TTTTTCCGTACTTAATGAAAACGG-3′ (XhoI restriction site is italicized). PCR was performed in a 50-μL reaction mixture containing genomic DNA (1 μg), forward and reverse primers (1 μM each), 10× Herculase buffer (5 μL), dNTP mixture (1 mM), and 5 U (1 μL) of Herculase-enhanced DNA polymerase. The reaction mixture was subjected to 30 cycles of amplification with an annealing temperature of 52 °C. The resulting PCR product was purified and digested with NdeI and XhoI restriction enzymes. The purified and digested PCR product was ligated with predigested pET22b(+) vector and transformed into electrocompetent *E. coli* DH5α cells. Selected clones were grown for minipreps and characterization by restriction mapping and DNA sequencing performed by Davis Sequencing Facility at the University of California, Davis.

Expression and purification of EfMan-I

Escherichia coli strains were cultured in LB rich medium (10 $g \cdot L^{-1}$ tryptone, 5 $g \cdot L^{-1}$ yeast extract, and 10 $g \cdot L^{-1}$ NaCl) supplemented with ampicillin (100 $\mu g \cdot mL^{-1}$). Overexpression of EfMan-I was achieved by inducing the *E coli* BL21 (DE3) cell culture with 0.15 mM of isopropyl-1-thio-D-galactopyranoside (IPTG) when the $OD_{600\ nm}$ of the culture reached 0.8–1.0 followed by incubation at 20 °C for 20 h.

Bacterial cells were harvested by centrifugation at 4 °C in a Sorvall Legend RT centrifuge with a hanging bucket rotor at 4000 r.p.m. for 2 h. Harvested cells were resuspended in lysis buffer (Tris/HCl buffer, 100 mM, pH 8.0 containing 0.1% Triton X-100) (20 mL for cells collected from 1 L cell culture). Lysozyme (100 $\mu g \cdot mL^{-1}$) and DNase I (5 $\mu g \cdot mL^{-1}$) were added to the cell resuspension. The resulting mixture was incubated at 37 °C for 1 h with shaking at 200 r.p.m. Cell lysate (supernatant) was obtained by centrifugation at 12 000 r.p.m. for 15 min. Purification was carried out by loading the supernatant onto a Ni^{2+}-NTA column pre-equilibrated with 10 column volumes of binding buffer (5 mM imidazole, 0.5 M NaCl, 50 mM Tris/HCl, pH 7.5). The column was washed with 10 column volumes of binding buffer and 10 column volumes of washing buffer (24 mM imidazole, 0.5 M NaCl, 50 mM Tris/HCl, pH 7.5). The target protein was eluted with Tris/HCl buffer (50 mM, pH 7.5) containing imidazole (200 mM) and NaCl (0.5 M). The fractions containing the purified enzymes were collected, dialyzed against Tris/HCl buffer (20 mM, pH 7.5) containing 10% glycerol with changing of dialysis buffer for three times, and stored at 4 °C.

Substrate specificity studies of EfMan-I

Typical enzymatic assays were performed in a 10-μL reaction mixture in MES buffer (100 mM, pH 6.0) containing substrate (10 mM) and EfMan-I (1.0 or 10 μg). Substrates used were as follows: Man α*p*NP, α2-mannobiose, α3-mannobiose, α6-mannobiose, Man_3, and Man_5. Reactions were allowed to proceed for 30 min, 18 h, or 24 h at room temperature (RM) or at 37 °C and were analyzed by TLC in a developing solvent (*n*-PrOH : H_2O : NH_4OH = 5 : 2 : 1 or *n*-PrOH : H_2O: NH_4OH = 3 : 2 : 1).

pH profile of EfMan-I

Standard enzymatic assays were carried out in duplicate in 384-well plates in a final volume of 20 μL in a buffer (100 mM) with a pH ranging from 3.0 to 9.0 containing Manα*p*NP (0.3 mM), $CaCl_2$ (4 mM), and EfMan-I (10.0 μg). Buffers used were as follows: citric acid-Na_2HPO_4, pH 3.0–4.0; NaOAc/HOAc, pH 4.5; MES, pH 5.0–6.5, and Tris/HCl pH 7.0–9.0. Reactions were incubated at 37 °C for 30 min and quenched by adding 40 μL of *N*-cyclohexyl-3-aminopropanesulfonic acid (CAPS) buffer (0.5 M, pH 10.5). The amounts of *para*-nitrophenolate formed were determined by measuring the $A_{405\ nm}$ of the reaction mixtures using a microplate reader. Reactions of Galβ*p*NP with an excess amount of β-galactosidase were used as controls.

Effects of ethylenediaminetetraacetic acid (EDTA) and metal Ions on EfMan-I

Ethylenediaminetetraacetic acid (10 mM), $CaCl_2$, or $MgCl_2$ were added at different concentrations (1, 2, 4, 8, 10, 20 mM) to reactions in MES buffer (100 mM, *p*H 6.0) to analyze their effects on the mannosidase activity of EfMan-I (10.0 μg) against Manα*p*NP. Reactions without the addition of EDTA or metal ions were used as a control. The concentrations of the substrates and other reaction conditions were the same as described above for the pH profile assays.

Kinetic studies of EfMan-I

Kinetic assays were carried out using three different substrates including Manα*p*NP, α2-mannobiose, and RNaseB. When Manα*p*NP was used as the substrate, the assays were carried out in duplicates in 384-well plates in a total volume of 20 μL in MES buffer (100 mM, pH 6.0) containing $CaCl_2$ (4 mM), Manα*p*NP at different concentrations in the range of 0.1–10 mM (0.1, 0.2, 0.4, 0.5, 1, 2, 5, 10 mM), and EfMan-I (14 μg). Reactions were incubated at 37 °C for 10 min and quenched by adding 40 μL of CAPS buffer (0.5 M, pH 10.5). The amounts of *para*-nitrophenolate formed were analyzed by a microplate reader and compared to a *p*NP standard curve. Apparent kinetic parameters were obtained by fitting the averages to the Michaelis–Menten equation using Grafit 5.0.

When α2-mannobiose was used as the substrate, reactions were performed in duplicate at 37 °C for 10 min in a total volume of 50 μL in MES buffer (100 mM, pH 6.0) containing varied concentrations of α2-mannobiose (0.1, 0.2, 0.5, 1, 2, 5, and 10 mM) and EfMan-I (6.2 nM). Reactions were quenched by incubating the reaction mixtures at 98 °C for 10 min. Precipitates were removed by centrifugation (11 000 ***g***, 5 min, 4 °C). The concentrations of mannose released were determined by a coupled enzyme assay as described [21]. Briefly, reactions were carried out at 25 °C in duplicate in a 384-well plate in the presence of Tris/HCl buffer (100 mM, pH 8.0), MES buffer (50 mM, 6.0), $MgCl_2$ (10 mM), $NADP^+$ (1 mM), ATP (1 mM), hexokinase from *S. cerevisiae* (0.75 U; Sigma-Aldrich, H4502-1KU), *E. coli* phosphomannose isomerase (0.75 U; Megazyme, E-PMIEC), phosphoglucose isomerase from baker's yeast (0.75 U; Sigma-Aldrich, P5381-1KU), and glucose-6-phosphate dehydrogenase from *L. mesenteroides* (0.75 U; Sigma-Aldrich, G9404-1KU). The absorbance of the NADPH formed was monitored by a microplate reader (Synergy HT; BioTek) at 340 nm in a 10-min interval, and the maximum reading was recorded and compared to the mannose standard curve.

To use RNase B as the substrate, the effective percentage of α1–2-mannose-containing RNase B (44%) was determined by complete releasing of α1–2-linked mannose from RNase B (0.8 mM) by incubating with EfMan-I (2.5 μM) at 37 °C for 4 h followed by quantification of the released mannose using coupled enzyme assay as described above. Kinetic studies using RNase B as the EfMan-I substrate were carried out at 37 °C for 10 min in a total volume of 50 μL in duplicate in the presence of MES buffer (100 mM, pH 6.0), EfMan-I (0.031 μM), and varied concentrations (0.1, 0.2, 0.3, 0.5, 1.0, and 2.5 mM) of RNase B. Reactions were quenched by incubating the reaction mixture at 98 °C for 10 min. Precipitates were removed by centrifugation (11 000 ***g***, 5 min, 4 °C). The concentrations of mannose released were determined similarly as described above using the coupled enzyme assay [21].

^{1}H NMR-based time course studies of EfMan-I using Manα*p*NP as the substrate

The assay was carried out in an NMR tube in 80% D_2O/H_2O solution (0.6 mL) containing phosphate buffer (10 mM, pH 6.0), Manα*p*NP (10 mM), $CaCl_2$ (4 mM), and EfMan-I (0.75 mg). NMR spectra (16 scans for each time point) were recorded at different reaction time points (0, 5, 10, 20, 30, 40, 50, 60, 90, and 120 min) in an 800 MHz Bruker Avance III spectrometer at a temperature of 310 K. The H_2O signal at 4.705 p.p.m. was suppressed.

MALDI-TOF MS analysis of N-glycans released from RNase B with or without EfMan-I treatment

RNase B or EfMan-I-treated RNase B (1 mg each) sample was denatured by adding 0.5% SDS and DTT (40 mM). The mixtures were incubated at 98 °C for 10 min and then at room temperature for 5 min. The glycans were released using 6 μg of peptide N-glycosidase F (PNGase F) by incubating the reaction mixtures at 37 °C for 24 h. The deglycosylated proteins were precipitated by adding threefold volume of cold ethanol and chilling the mixtures at −80 °C for 2 h. The mixtures were then centrifuged at 15 000 r.p.m. for 20 min, and the supernatants containing the glycans were dried in speed vacuum for matrix-assisted laser desorption/ionization-time of flight (MALDI-TOF) mass spectrometry (MS) analysis.

High-performance liquid chromatography (HPLC) and MALDI-TOF MS analyses of 2-aminobenzamide (2-AB)-labeled N-glycans released from RNase B with or without EfMan-I treatment

2-aminobenzamide solution (A) was prepared by adding 88 mg of 2-AB to 1 mL of DMSO/AcOH (7 : 3 by volume). The solution was stored at −20 °C. Sodium cyanoborohydride solution (B) was freshly prepared by adding 64 mg of $NaCNBH_3$ to 1 mL of a solution mixture of DMSO/AcOH (7 : 3 by volume). To a dried free reducing glycan sample (0.01–1 mg), solution A (5–50 μL) and an equal volume of solution B were added. The mixture was heated at 65 °C for 2 h. A 10-fold volume of acetonitrile was then added to precipitate the glycan-2AB conjugates. The mixture was cooled down at −20 °C for 1 h and centrifuged at 13 000 r.p.m. for 2 min. The precipitate was collected and dissolved in H_2O (100–1000 μL). The obtained mixture was centrifuged at 13 000 r.p.m. for 2 min. The supernatant was collected and diluted, and the glycan-2AB conjugates were analyzed using HPLC with an AdvanceBio Glycan Map column (Agilent) using a slow gradient of Solvent A (ammonium formate, 100 mM, pH 4.5) and Solvent B (acetonitrile) and monitoring at $A_{254\ nm}$.

Crystallization of EfMan-I

EfMan-I in Tris/HCl buffer (10 mM, pH 7.5) was concentrated to 10 mg·mL^{-1} using centrifugal filter units (EMD Millipore, Billerica, MA, USA) and crystallized by sitting drop vapor diffusion in a 1 : 1 ratio of protein and reservoir solution at 21 °C. The reservoir solution contained NaOAc (0.1 M, pH 4.5) and NaH_2PO_4 (0.8 M)/K_2HPO_4 (1.2 M). The crystals were briefly soaked in the reservoir solution that also contained 30% glycerol prior to flash cooling in liquid nitrogen for X-ray diffraction data collection.

Data collection, model building, and refinement

X-Ray diffraction data were collected at Stanford Synchrotron Radiation Lightsource (SSRL) beamline 12–2 at

100 K. Diffraction data were indexed and integrated with XDS [35], and then scaled with XSCALE [36]. A complete diffraction data set was collected to 2.15 Å resolution with an R_{merge} of 9.6%. Data collection and structure refinement statistics are given in Table S1. The crystals belong to the orthorhombic space group $C222_1$ with unit cell parameters: a = 163.35 Å, b = 169.00 Å, c = 258.52 Å, α = β = γ = 90°, which contain four monomers per asymmetric unit (V_M = 2.70 Å^3/Da, solvent = 54.48%) [37]. The EfMan-I structure was solved by molecular replacement applying a model of the previously solved α-mannosidase structure from *S. pneumoniae* (PDBID: 5swi) using the program PHASER [38]. Atomic model building was carried out with the molecular graphics program COOT [39,40]. The structure was refined with the program REFMAC5 [41] part of the CCP4 package [42]. Noncrystallographic symmetry restraints were included during refinement. The final *R*-factor (15.5%) and *R*-free (18.9%) along with the quality of the models are listed in Table S1.

Results and Discussions

Cloning and purification of EfMan-I

The full-length gene of *EF2217* (2142 bp encoding 713 aa) was cloned from the genomic DNA of *E. faecalis* V583 into pET22b(+) vector. EfMan-I was expressed as a C-His$_6$-tagged fusion protein. Protein sequence alignment (Fig. S1 and Table S2) showed that EfMan-I shared 46.4% identity with SpGH92 from *S. pneumoniae* TIGR4 [22]. It also shared 34.1% and 32.1% identities, respectively, with Bt2199 and Bt3990, which are two α1–2-mannosidases from *B. thetaiotaomicron* VPI-5482 [21].

EfMan-I was expressed at 20 °C as a soluble form in *E. coli* BL21 (DE3) cells by induction using 0.15 mM of IPTG. Under these expression conditions, 85 mg of purified protein was routinely obtained from 1 L of *E. coli* cell culture by one-step nickel-nitrilotriacetic acid (Ni^{2+}-NTA) affinity chromatography. This expression level was comparable or higher than that reported for Bt2199 and Bt3990 (> 500 nM or 41 mg per liter culture) [21].

SDS/PAGE analysis (Fig. 1) indicated that the apparent molecular weight of purified EfMan-I was about 73 kDa, which was smaller than the calculated molecular weight (82.7 kDa). Nevertheless, N-terminal amino acid sequencing (Table S3) showed an intact N terminus. The efficient one-step Ni2+-NTA affinity chromatography process indicated the presence of the C-His6-tag in the recombinant EfMan-I introduced by cloning.

Substrate specificity studies of EfMan-I

Substrate specificity studies of EfMan-I (Fig. 2) in MES buffer (100 mM, pH 6.0) using *para*-nitrophenyl-α-D-mannopyranoside (Manα*p*NP), α2-mannobiose, α3-mannobiose, α6-mannobiose, D-mannotriose (Man_3), or 3α,6α-mannopentaose (Man_5) as the substrate showed that α2-mannobiose was completely hydrolyzed by EfMan-I, while Manα*p*NP was partially hydrolyzed and other compounds tested were not hydrolyzed by EfMan-I in a 30-min time frame. However, after a prolonged incubation time of 24 h, Manα*p*NP was completely hydrolyzed to form mannose and *p*NP (Fig. 2, lane 2). It was interesting to note that both α3-mannobiose and α6-mannobiose were also partially hydrolyzed by EfMan-I to form mannose (Fig. 2, lanes 6 and 8) and the hydrolytic activity of EfMan-I toward α3-mannobiose was slightly higher than that toward α6-mannobiose. Nevertheless, oligomannoses Man_3 and Man_5 were not suitable substrates for EfMan-I and they remained intact even after a long (18 h) incubation period with 10-fold more enzyme (10 μg) at room temperature or at 37 °C (Fig. 2C). This suggested that EfMan-I only catalyzed unbranched α1–3- and α1–6-linked mannose with low efficiency. The weak activity on cleaving α1–6-linked mannose on an unbranched mannoside chain is similar to a reported soil bacterium *Solitalea canadensis*α-mannosidase (Sca6Man4191) [43]. Therefore, EfMan-I is an α-mannosidase with high efficiency in catalyzing the cleavage of α1–2-linked mannose and with weak activity toward unbranched α1–3- and α1–6-linked mannosides.

pH Profile and metal ion effects on EfMan-I

As shown in Fig. 3A, EfMan-I preferred a mild acidic reaction condition and its optimum activity was

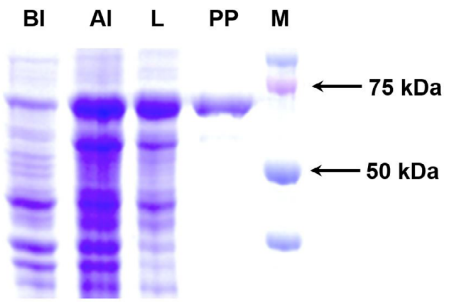

COLOR

Fig. 1. SDS/PAGE (10% Tris-Glycine gel) analysis for the expression and the purification of EfMan-I. Lanes: BI, whole-cell extract before induction; AI, whole-cell extract after induction; L, lysate after induction; PP, Ni^{2+}-NTA column purified protein; M, protein markers (Bio-Rad precision Plus Protein Standards, 10–250 kDa).

COLOR

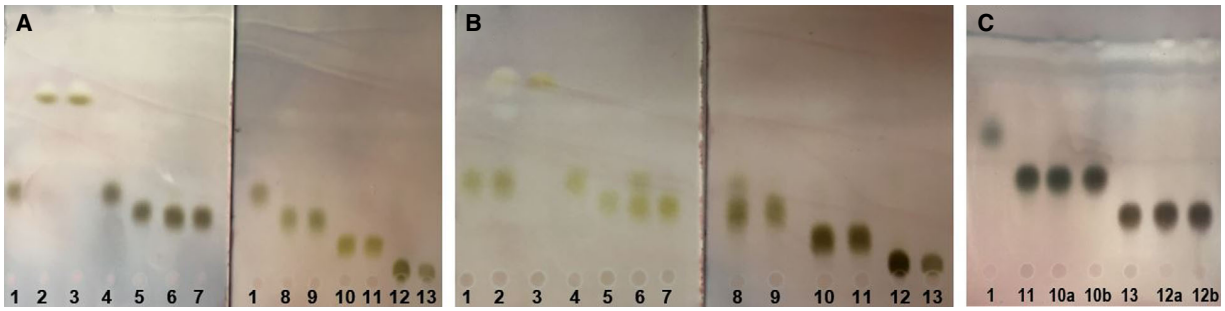

Fig. 2. Substrate specificity studies of EfMan-I by TLC analysis with reactions carried out at 37 °C for (A) 30 min or (B) 24 h in the presence of EfMan-I (1.0 μg) (developing solvent used was *n*-PrOH : H_2O : $NH_3{\cdot}H_2O$ = 5 : 2 : 1, by volume). For (C), reactions were carried out in the presence of EfMan-I (10 μg) at room temperature (for 10a and 12a) or at 37 °C (for 10b and 12b) for 18 h (developing solvent used was *n*-PrOH:H_2O:$NH_3{\cdot}H_2O$ = 3 : 2 : 1, by volume). Lanes: 1, mannose; 2, Manα*p*NP in the presence of EfMan-I; 3, Manα*p*NP; 4, α2-mannobiose in the presence of EfMan-I; 5, α2-mannobiose; 6, α3-mannobiose in the presence of EfMan-I; 7, α3-mannobiose; 8, α6-mannobiose in the presence of EfMan-I; 9, α6-mannobiose; 10, Man_3 in the presence of EfMan-I; 11, Man_3; 12, Man_5 in the presence of EfMan-I; 13, Man_5.

observed at pH 6.0. Medium activity was observed at pH 6.5 and in a pH range of 5.0–5.5. EfMan-I activity decreased drastically when the pH was at or below 4.5, or at or above 7.0. The effects of a metal ion such as Ca^{2+} or Mg^{2+} and a chelating agent EDTA on the activity of EfMan-I in catalyzing the cleavage of Man-α*p*NP were examined at pH 6.0. As shown in Fig. 3B, the activity of EfMan-I was abolished by the addition of EDTA, while it was not significantly affected by the addition of Ca^{2+} or Mg^{2+} for up to 20 mM, indicating that a pre-existing metal ion bond to EfMan-I was important for its catalytic activity.

Kinetic studies of EfMan-I

Three substrates including Manα*p*NP, α2-mannobiose, and RNaseB were used to determine the apparent kinetics data for EfMan-I. As shown in Table 1, Manα*p*NP was the least efficient substrate among the three. Using Manα*p*NP as the substrate, the catalytic efficiency (k_{cat}/K_M) of EfMan-I was 4.7×10^{-2} $s^{-1}{\cdot}mM^{-1}$ or 2.82 $min^{-1}{\cdot}mM^{-1}$ (Fig. S2). In comparison, the catalytic efficiencies of Bt2199 and Bt3990 were 0.84 and 1.3 $min^{-1}{\cdot}mM^{-1}$, respectively [21]. EfMan-I was the most efficient in catalyzing the cleavage of α1–2-mannosyl linkage in α2-mannobiose with a catalytic efficient (k_{cat}/K_M) of 58 s^{-1} mM^{-1} (Fig. S3), which was more than 1200-fold higher than that of Manα*p*NP. The difference was contributed by both a higher turnover number (367-folder) and an improved binding (3.5-fold) for α2-mannobiose. RNase B was also an efficient substrate with a catalytic efficient (k_{cat}/K_M) of 22 $s^{-1}{\cdot}mM^{-1}$ (Fig. S4), which was about 468-fold higher than that of Manα*p*NP.

^{1}H NMR-based time course studies of EfMan-I using ManαpNP as the substrate

^{1}H NMR-based time course studies (Fig. S5) showed that EfMan-I-catalyzed reaction follows an inversion mechanism similar to that described for Bt2199 and Bt3990 previously [21]. For example, β-mannose was observed as the main product of EfMan-I from Man-α*p*NP substrate in the first 10 min. With a longer reaction time and the accumulation of β-mannose product, α-mannose appeared quickly due to a quick mutarotation process.

MALDI-TOF MS analysis of N-glycans released from RNase B with or without EfMan-I treatment

In order to test the activity of EfMan-I in catalyzing the cleavage of α1–2-mannose from high-mannose N-glycans on glycoprotein substrates, RNase B, a glycoprotein containing a single N-glycosylation, was treated with EfMan-I. The N-glycans of RNase B with or without EfMan-I-treatment were then released by PNGase F [44,45] and analyzed by MALDI-TOF MS [46]. As shown in Fig. S6, without EfMan-I-treatment (RNase B control), $Man_5GlcNAc_2$, $Man_6GlcNAc_2$, $Man_7GlcNAc_2$, $Man_8GlcNAc_2$, and $Man_9GlcNAc_2$ were observed as the N-glycans released from RNase B by PNGase F (Fig. S6A). In comparison, with EfMan-I treatment, all $Man_{6-9}GlcNAc_2$ N-glycan structures were converted to $Man_5GlcNAc_2$ (Fig. S6B). These results confirmed that EfMan-I was specific for catalyzing the cleavage of α1–2-linked mannose residues on high-mannose-type N-glycans on glycoproteins.

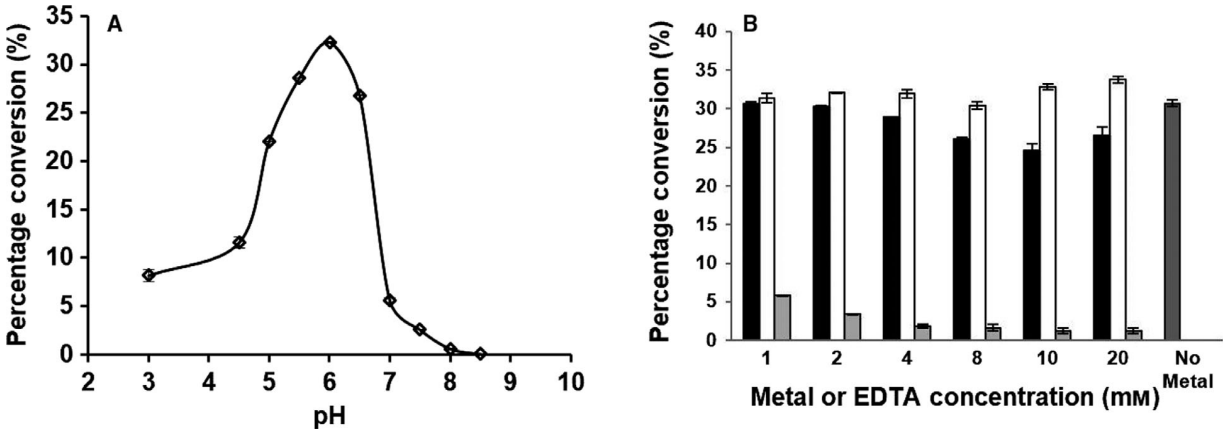

Fig. 3. pH Profile (A) as well as metal ion and EDTA effects (B) on EfMan-I using Manα*p*NP as the substrate. For A, buffers used were as follows: citric acid-Na_2HPO_4, pH 3.0–4.0; NaOAc/HOAc, pH 4.5; MES, pH 5.0–6.5, and Tris/HCl pH 7.0–9.0. For B, Black columns, $MgCl_2$; white columns, $CaCl_2$; light gray columns, EDTA; dark gray column, no metal and no EDTA control.

Table 1. Apparent kinetics data of EfMan-I.

Acceptor	k_{cat} (s^{-1})	K_M (mM)	k_{cat}/K_M ($s^{-1}\cdot$ mM $^{-1}$)
Manα*p*NP	0.49 ± 0.03	11 ± 1.7	4.7×10^{-2}
α2-mannobiose	$(1.8 \pm 0.1) \times 10^2$	3.1 ± 0.3	58
RNase B	42 ± 3	1.9 ± 0.2	22

HPLC and MALDI-TOF MS analyses of 2-AB-labeled N-glycans released from RNase B with or without EfMan-I treatment

To quantitatively analyze the activity of EfMan-I against glycoprotein, the N-glycans of RNase B with or without EfMan-I treatment were released and labeled with 2-AB [47]. As shown in Figs 4 and Fig. S7, without EfMan-I treatment, 2-AB-labeled $Man_5GlcNAc_2$ (~ 50%), $Man_6GlcNAc_2$ (~ 37%), and $Man_{7-9}GlcNAc_2$ (~ 13%) were observed for the RNase B sample. With EfMan-I treatment, all $Man_{6-9}GlcNAc_2$ on RNase B were converted to $Man_5GlcNAc_2$.

Crystal structure of EfMan-I

EfMan-I crystallized in Space group $C222_1$ with four molecules per asymmetric unit. However, given the limited amount of surface area buried between monomers in the crystal packing, EfMan-I is most likely monomeric in solution. The electron density, at 2.15 Å resolution, clearly defined residues 1–712 in all four subunits in the asymmetric unit. The overall structure of EfMan-I contains two domains; an N-terminal 14-stranded antiparallel β-sandwich domain and a larger C-terminal helical domain with $(\alpha/\alpha)_6$ topology (Fig. 5A). This two-domain architecture is seen in homologous GH92 α-mannosidases [21,22,49] and other glycosidases [23,50–52]. The N-terminal β-sandwich displays some similarities to non-catalytic β-sandwich domains found in larger GH38 family glycosidases like Drosophila Golgi retaining α-mannosidases [53] and bovine lysosomal α-mannosidase [54]. In EfMan-I and in homologous GH92 family α-mannosidases, the active site lies in a cleft between the N-terminal β-sandwich domain and the C-terminal $(\alpha/\alpha)_6$ domain. It is interesting to note that the two-domain glycosidases are typically exo-glycosidases, while glycosidases with only a single $(\alpha/\alpha)_6$ domain are typically endo-glycosidases [55,56], suggesting the β-sandwich domain restricts the active site to only terminal sugars.

The active site is located close to the center of the $(\alpha/\alpha)_6$ domain, and the N-terminal β-sandwich domain helps to shape part of the active site. Specifically, Trp68 of the N-terminal domain lies above the active site and helps in binding substrate and substrate analogs as observed in other α-mannosidases [21,22]. Electron density clearly reveals that the active site of all four subunits in the asymmetric unit contains a bound metal with an octahedral coordination geometry. Although no divalent cations were included in protein purification or crystallization, the metal was modeled as a calcium ion because other GH92 family α-mannosidases require calcium for activity and calcium ions were observed in their structures [21,22,49]. The presence of a calcium ion in the crystal structure can explain the activity of EfMan-I observed without the addition of an external metal cation. The calcium is

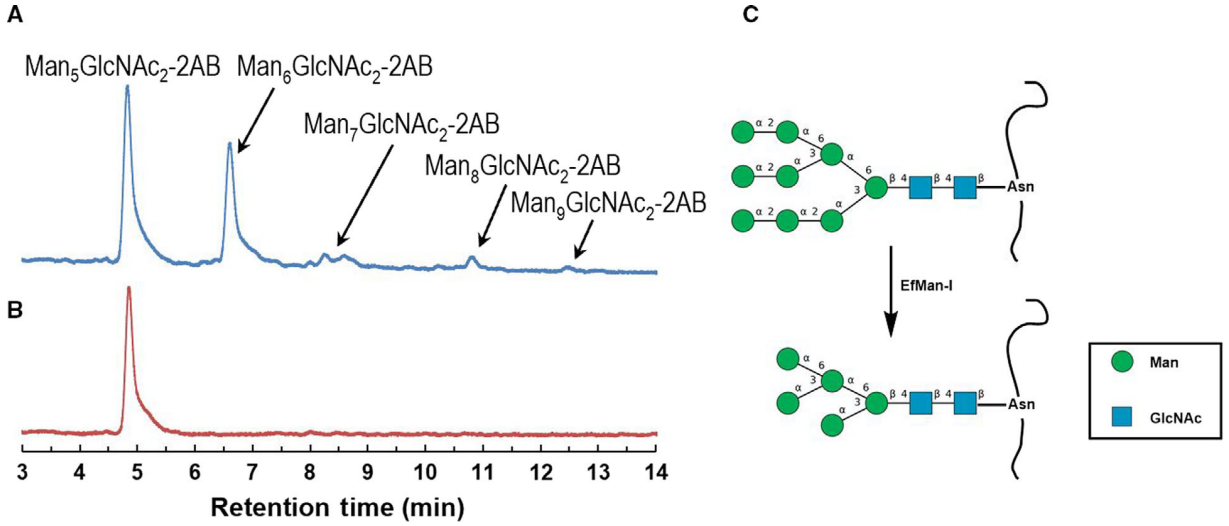

Fig. 4. HPLC analysis of 2-AB-labeled high-mannose N-linked glycans from RNase B without (A) and with (B) EfMan-I treatment; and schematic illustration of the reaction catalyzed by EfMan-I (C) [48].

coordinated by the side chains of Asn562 (2.6 Å), Gln563 (2.4 Å), and Asp604 (2.4 Å) together with two water molecules (2.6 and 2.7 Å) (Fig. 5B). The sixth ligand comes from a 'tube' of electron density, which was modeled as glycerol since it was added as a cryoprotectant. Additionally, electron density was observed near the calcium ion in the active site in all four monomers in the crystallographic asymmetric unit, which was also modeled as glycerol (Fig. 5B). Glycerol was also observed in the active site of other α-mannosidases (see below) [21–23].

Strong electron density was also observed adjacent to Asn20 that was modeled as a potassium ion since it was present in the crystallization conditions (Fig. 5C). Placement of sodium, also present in the crystallization conditions, resulted in strong positive difference electron density after subsequent rounds of refinement, confirming the likelihood of a more electron dense potassium ion at this location. Ligation distances and geometry are also similar to potassium ions in other protein structures [57]. The potassium ion binds on the surface of the protein at the interface between the N-terminal and C-terminal domains, where Asn20 Oδ1 coordinates (2.7 Å) together with carbonyl oxygens from Thr597 (2.8 Å) and Tyr599 (2.7 Å) (Fig. 5C). Two water molecules finish the coordination sphere resulting in a square pyramidal geometry. Although this potassium ion is also observed in all four monomers of the asymmetric unit, it is likely not directly involved in catalysis because it binds on the peripheral of the protein over 13 Å from the active site. However, the presence of a potassium ion situated at the interface between the two domains suggests the ion may play a role in helping position the proper orientation between the domains to shape the active site. This hypothesis still remains to be tested in future studies. In comparison, a sodium ion was modeled in a similar position in the *B. thetaiotaomicron* α-mannosidase Bt2199 (PDBID 2ww2) [21]. In Bt2199 structure, the ion is octahedrally coordinated by main chain carbonyl oxygens of Ser40, Tyr643, Gly645, and Asp648 with two waters completing the octahedral coordination.

Comparison of EfMan-I structure to other α-mannosidases

The closest EfMan-I homolog with a known structure is an α-mannosidase from human pathogen *S. pneumoniae* (SpGH92) [22], which has 47% sequence identity. The two crystal structures superimpose with an rmsd of 1.07 Å over 672 equivalent α-carbons (Fig. 6A). The only major deviation is in a loop centered around residue Met359 near the active site (Fig. 6A). In the EfMan-I structure, the loop adopts a conformation that closes in on the active site. However, in the SpGH92 structure, one of the four monomers in the asymmetric unit adopts two conformations of the loop, one resembles more closely the conformation of EfMan-I. The three other SpGH92 monomers in the asymmetric unit only adopt one conformation extending away from the active site as observed in Fig. 6A. The different conformations between these two structures that help shape the active-site pocket may be important in substrate binding specificity. However, the corresponding loop in

COLOR

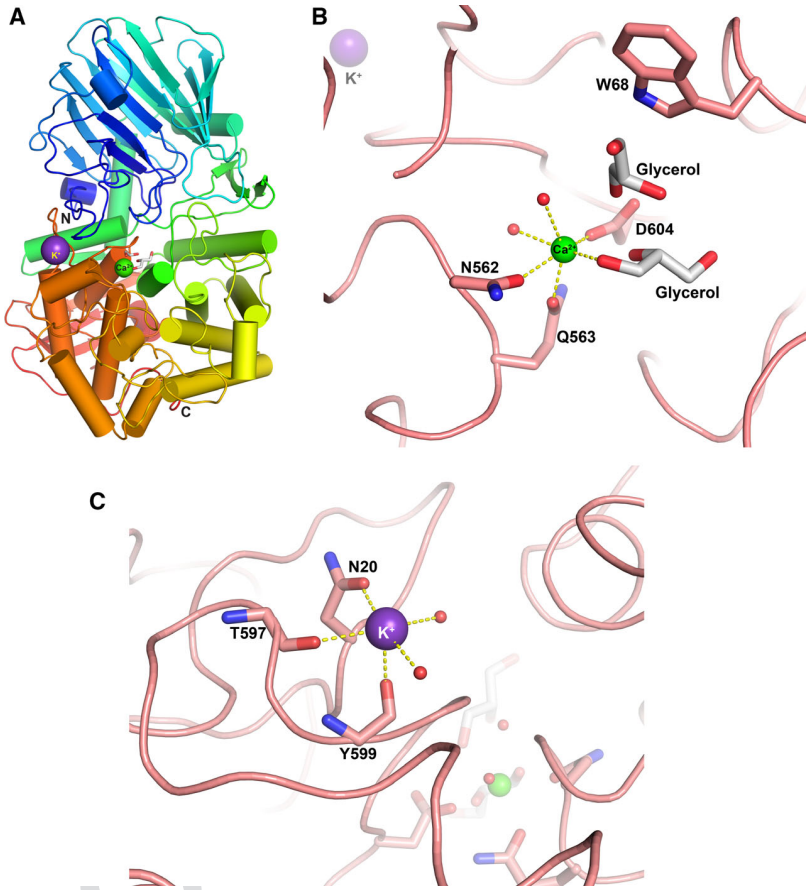

Fig. 5. Overall structure of EfMan-I monomer (A), its active site (B), and potassium-binding site (C). Ribbon drawing of EfMan-I colored by a rainbow gradient according to sequence number, starting with blue at the N terminus, and ending with red at the C terminus. The active site is identified by the Ca^{2+} ion shown as a green sphere together with glycerol molecules (sticks) that interact with the Ca^{2+} ion shown as a green sphere together with the coordination ligands (water molecule ligands shown as smaller red spheres). Yellow dashed lines represent coordination interactions (between 2.6–2.9 Å). The two glycerol molecules modeled in the active site are shown as sticks with white-colored carbon atoms. A K^+ ion binds to the peripheral of the $(\alpha/\alpha)_6$ domain is shown as a purple-colored sphere together with the coordination ligands (water molecule ligands shown as smaller red spheres). Only main chain atoms are shown for Thr597 and Tyr599.

the α-mannosidases from *B. thetaiotaomicron* (the next closest homolog at 32–34% identity) displays (not shown) this loop in a closed conformation similar to EfMan-I [21,49].

The active sites of the EfMan-I and SpGH92 structures are very similar with homologous residues coordinating the calcium ion (Fig. 6B). In the EfMan-I structure, two glycerol molecules are observed in the active site, one is involved in coordinating the calcium ion (−1 subsite), and another glycerol stacks up against Trp68 (+1 subsite). In the SpGH92 structure (PDBID 5swi), crystals were soaked with α1–2-mannobiose, which was hydrolyzed and only mannose was observed to bind to the +1 subsite location in a similar location to the secondary glycerol of EfMan-I (Fig. 6B). The −1 subsite of SpGH92 was occupied by a glycerol molecule that coordinated the calcium ion as also observed in EfMan-I. Previous α-mannosidase kinetic and structural analyses have proposed a general acid–base mechanism and identified catalytic residues [21]. These residues map to Glu494 and Asp604 in serving as the respective general acid and general base catalytic residues in EfMan-I (Fig. 6B). It is interesting to note that Asp604 also serves as a calcium ligand in the active site.

Several crystal structures have been determined for GH92 family α-mannosidases from the human gut microbe *B. thetaiotaomicron* (Bt) with various substrates and inhibitors bound in the active site [21,49]. These include Bt2119, Bt3990, Bt3130, and Bt3965, all of which have similar structures to EfMan-I. Bt3990, which has a 32% sequence identity to EfMan-I, superimposes onto EfMan-I with an rmsd of 1.29 Å over 696 equivalent α-carbons. The structure of Bt3990 was determined with a nonhydrolyzable disaccharide of thio-α2-mannobioside (PDBID 2ww3). Superposition of this active site onto EfMan-I is shown in Fig. 7, which reveals they are very similar. The glycerol in EfMan-I that coordinates the calcium ion superimposes more on the –1 subsite saccharide, while the second glycerol occupies a position in between the two saccharides of the thio-α2-mannobioside substrate analog in Bt3990. The only main difference in the active sites is the movement of Asn601 in Bt3990. The equivalent residue (Asn562) of EfMan-I coordinates the calcium ion, while in Bt3990, it shifts down and a water

COLOR

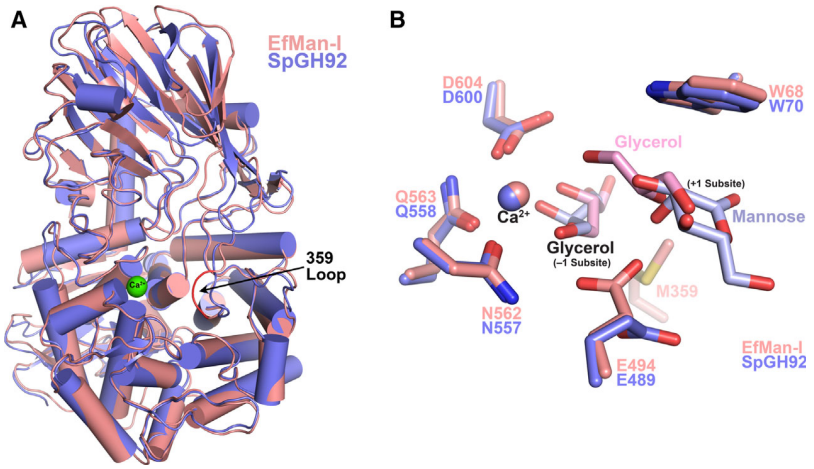

Fig. 6. Superposition of EfMan-I (salmon color) and SpGH92 (slate blue) structures (A) and their active sites (B). They superimpose with an rmsd of 1.07 Å over 672 equivalent α-carbons. Calcium ions in the active site are shown as green spheres, and the 359 loop near the active site is highlighted in bright red color for EfMan-I. The side chains of residues that coordinate the calcium ion are shown along with ordered glycerol molecules found in both mannosidase structures. Note that in each structure a glycerol coordinates the calcium ion and in the EfMan-I structure, another glycerol binds in a similar location to mannose observed in SpGH92, which is 3.4 Å below the indole ring of Trp68. Glu494 and Asp604 are proposed to be the respective general acid and general base in catalysis.

molecule occupies the vacated coordination space. However, in another Bt3990 structure complexed with the inhibitor swainsonine (PDBID 2ww0), Asn601 does indeed coordinate the calcium ion similar to Asn562 of EfMan-I.

In conclusion, a new α1–2-mannosidase from *E. faecalis* (EfMan-I) has been identified and characterized. It has been found to catalyze the cleavage of α1–2-linked mannose residues highly efficiently from not only oligomannosides but also glycoproteins containing high-mannose-type N-glycans using ribonuclease B as a model glycoprotein. It is an inverting glycosidase similar to two characterized GH92 α1–2-mannosidases (Bt3990 and Bt2199) from *B. thetaiotaomicron* VPI-5482. The crystal structure of EfMan-I reveals a similar fold to other GH92 α-mannosidases and identifies residues in the active site that ligate the essential calcium ion and are involved in substrate binding and catalysis. Ordered glycerol molecules, used for cryoprotection, bind in the active site with one molecule ligating to the active-site calcium ion. An unexpected potassium ion was observed bridging two domains near the active site. With a good expression level in *E. coli*, high activity and high selectivity on cleaving α1–2-linked mannose residues in oligomannose structures including those attached to glycoproteins, the newly characterized EfMan-I is a powerful tool for *in vitro* enzymatic modification of high-mannose-type N-glycans on glycoproteins. Its characterization is also helpful for better understanding the use of host or dietary glycoproteins as nutrients by *E. faecalis*, a Gram-positive commensal bacterium and an opportunistic pathogen that can cause health care-associated infection (HAI).

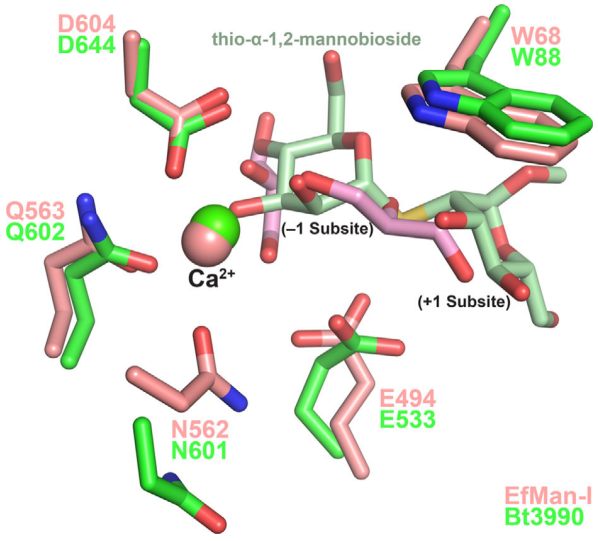

COLOR

Fig. 7. Superposition of EfMan-I (salmon color) and Bt3990 (green) active sites. The side chains of residues that coordinate the calcium ion are shown along with ordered glycerol molecules found in EfMan-I structure (pink-colored carbon atoms) and the substrate analog thio-α2-mannobioside in Bt3990 (pale-green carbon atoms). Location of the calcium ion is shown by spheres with colors corresponding to their respective active sites.

Acknowledgements

The authors would like to acknowledge the collaboration of Karen A. McDonald, Somen Nandi, Carlito B. Lebrilla, and their coworkers on the *in vitro* enzymatic glycoprotein glycan modulation project, providing helpful discussion and assistance. We would also like to thank Prof. Peng G. Wang's group at Georgia State University for providing the plasmid for expressing PNGase F in *E. coli*. The atomic coordinates and structure factors have been deposited in the Protein Data Bank, PDBID 6dwo (https://www.rcsb.org).

Author contributions

XC and AJF conceived and supervised the study; YL, RL, AJF, and XC designed experiments; YL, RL, HY, XS, JW, and AJF performed experiments; all authors analyzed data; YL, RL, AJF and XC wrote the manuscript with the input from all authors.

Funding

This work was supported by the United State Defense Threat Reduction Agency (HDTRA1-15-1-0054). Use of the SSRL, SLAC National Accelerator Laboratory, was supported by the U.S. Department of Energy, Office of Science, Office of Basic Energy Sciences under Contract No. DE-AC02-76SF00515. The SSRL Structural Molecular Biology Program is supported by the DOE Office of Biological and Environmental Research, and by the National Institutes of Health, National Institute of General Medical Sciences (including P41GM103393). The contents of this publication are solely the responsibility of the authors and do not necessarily represent the official views of DTRA, NIGMS, or NIH. The funding sponsors had no role in the design of the study; in the collection, analyses, or interpretation of data; in the writing of the manuscript; and in the decision to publish the results.

References

1 Jefferis R (2016) Posttranslational modifications and the immunogenicity of biotherapeutics. *J Immunol Res Article* **2016**, 1–15.

2 Yang Q and Wang LX (2017) Chemoenzymatic glycan remodeling of natural and recombinant glycoproteins. *Methods Enzymol* **597**, 265–281.

3 Seeberger PH and Cummings RD (2015) Glycans in biotechnology and the pharmaceutical industry. In Essentials of Glycobiology (Varki A, Cummings RD and Esko JD *et al*. eds), pp. 729–741, Cold Spring Harbor Laboratory Press, Cold Spring Harbor, NY.

4 Li H and d'Anjou M (2009) Pharmacological significance of glycosylation in therapeutic proteins. *Curr Opin Biotechnol* **20**, 678–684.

5 Walsh G and Jefferis R (2006) Post-translational modifications in the context of therapeutic proteins. *Nat Biotechnol* **24**, 1241–1252.

6 Sola RJ and Griebenow K (2010) Glycosylation of therapeutic proteins: an effective strategy to optimize efficacy. *BioDrugs* **24**, 9–21.

7 Wang LX and Lomino JV (2012) Emerging technologies for making glycan-defined glycoproteins. *ACS Chem Biol* **7**, 110–122.

8 Witte K, Sears P, Martin R and Wong CH (1997) Enzymatic glycoprotein synthesis: preparation of ribonuclease glycoforms via enzymatic glycopeptide condensation and glycosylation. *J Am Chem Soc* **119**, 2114–2118.

9 Wang L-X and Amin MN (2014) Chemical and chemoenzymatic synthesis of glycoproteins for deciphering functions. *Chem Biol* **21**, 51–66.

10 Gamblin DP, Scanlan EM and Davis BG (2009) Glycoprotein synthesis: an update. *Chem Rev* **109**, 131–163.

11 Chalker JM, Bernardes GJ and Davis BG (2011) A "tag-and-modify" approach to site-selective protein modification. *Acc Chem Res* **44**, 730–741.

12 Hamilton SR, Davidson RC, Sethuraman N, Nett JH, Jiang Y, Rios S, Bobrowicz P, Stadheim TA, Li H, Choi BK *et al*. (2006) Humanization of yeast to produce complex terminally sialylated glycoproteins. *Science* **313**, 1441–1443.

13 Li H, Sethuraman N, Stadheim TA, Zha D, Prinz B, Ballew N, Bobrowicz P, Choi BK, Cook WJ, Cukan M *et al*. (2006) Optimization of humanized IgGs in glycoengineered *Pichia pastoris*. *Nat Biotechnol* **24**, 210–215.

14 Jacobs PP, Geysens S, Vervecken W, Contreras R and Callewaert N (2009) Engineering complex-type N-glycosylation in *Pichia pastoris* using GlycoSwitch technology. *Nat Protoc* **4**, 58–70.

15 Yamamoto N, Tanabe Y, Okamoto R, Dawson PE and Kajihara Y (2008) Chemical synthesis of a glycoprotein having an intact human complex-type sialyloligosaccharide under the Boc and Fmoc synthetic strategies. *J Am Chem Soc* **130**, 501–510.

16 Fischer BE and Dorner F (1998) Recombinant coagulation factor IX: glycosylation analysis and *in vitro* conversion into human-like sialylation pattern. *Thromb Res* **89**, 147–150.

17 Stanley P, Taniguchi N and Aebi M (2015) N-Glycans. In Essentials of Glycobiology (Varki A, Cummings RD and Esko JD *et al*. eds), pp. 99-111, Cold Spring Harbor Laboratory Press, Cold Spring Harbor, NY.

18 Takahashi M, Kuroki Y, Ohtsubo K and Taniguchi N (2009) Core fucose and bisecting GlcNAc, the direct

modifiers of the N-glycan core: their functions and target proteins. *Carbohydr Res* **344**, 1387–1390.
19 Strasser R (2016) Plant protein glycosylation. *Glycobiology* **26**, 926–939.
20 Xiang Y, Karaveg K and Moremen KW (2016) Substrate recognition and catalysis by GH47 alpha-mannosidases involved in Asn-linked glycan maturation in the mammalian secretory pathway. *Proc Natl Acad Sci USA* **113**, E7890–E7899.
21 Zhu Y, Suits MD, Thompson AJ, Chavan S, Dinev Z, Dumon C, Smith N, Moremen KW, Xiang Y, Siriwardena A *et al.* (2010) Mechanistic insights into a Ca^{2+}-dependent family of alpha-mannosidases in a human gut symbiont. *Nat Chem Biol* **6**, 125–132.
22 Robb M, Hobbs JK, Woodiga SA, Shapiro-Ward S, Suits MD, McGregor N, Brumer H, Yesilkaya H, King SJ and Boraston AB (2017) Molecular characterization of N-glycan degradation and transport in *Streptococcus pneumoniae* and its contribution to virulence. *PLoS Pathog* **13**, e1006090.
23 Tiels P, Baranova E, Piens K, De Visscher C, Pynaert G, Nerinckx W, Stout J, Fudalej F, Hulpiau P, Tannler S *et al.* (2012) A bacterial glycosidase enables mannose-6-phosphate modification and improved cellular uptake of yeast-produced recombinant human lysosomal enzymes. *Nat Biotechnol* **30**, 1225–1231.
24 Maruyama Y, Nakajima T and Ichishima E (1994) A 1,2-alpha-D-mannosidase from a *Bacillus sp.*: purification, characterization, and mode of action. *Carbohydr Res* **251**, 89–98.
25 Henrissat B (1991) A classification of glycosyl hydrolases based on amino acid sequence similarities. *Biochem J* **280** (Pt 2), 309–316.
26 Henrissat B and Bairoch A (1993) New families in the classification of glycosyl hydrolases based on amino acid sequence similarities. *Biochem J* **293** (Pt 3), 781–788.
27 Henrissat B and Bairoch A (1996) Updating the sequence-based classification of glycosyl hydrolases. *Biochem J* **316** (Pt 2), 695–696.
28 Koropatkin NM, Cameron EA and Martens EC (2012) How glycan metabolism shapes the human gut microbiota. *Nat Rev Microbiol* **10**, 323–335.
29 Paulsen IT, Banerjei L, Myers GS, Nelson KE, Seshadri R, Read TD, Fouts DE, Eisen JA, Gill SR, Heidelberg JF *et al.* (2003) Role of mobile DNA in the evolution of vancomycin-resistant *Enterococcus faecalis*. *Science* **299**, 2071–2074.
30 Goh HMS, Yong MHA, Chong KKL and Kline KA (2017) Model systems for the study of Enterococcal colonization and infection. *Virulence* **8**, 1525–1562.
31 Sahm DF, Kissinger J, Gilmore MS, Murray PR, Mulder R, Solliday J and Clarke B (1989) *In vitro* susceptibility studies of vancomycin-resistant *Enterococcus faecalis*. *Antimicrob Agents Chemother* **33**, 1588–1591.
32 Roberts G, Tarelli E, Homer KA, Philpott-Howard J and Beighton D (2000) Production of an endo-beta-N-acetylglucosaminidase activity mediates growth of *Enterococcus faecalis* on a high-mannose-type glycoprotein. *J Bacteriol* **182**, 882–890.
33 Collin M and Fischetti VA (2004) A novel secreted endoglycosidase from *Enterococcus faecalis* with activity on human immunoglobulin G and ribonuclease B. *J Biol Chem* **279**, 22558–22570.
34 Bohle LA, Mathiesen G, Vaaje-Kolstad G and Eijsink VG (2011) An endo-beta-N-acetylglucosaminidase from *Enterococcus faecalis* V583 responsible for the hydrolysis of high-mannose and hybrid-type N-linked glycans. *FEMS Microbiol Lett* **325**, 123–129.
35 Kabsch W (2010) Xds. *Acta Crystallogr D Biol Crystallogr* **66**, 125–132.
36 Kabsch W (2010) Integration, scaling, space-group assignment and post-refinement. *Acta Crystallogr D Biol Crystallogr* **66**, 133–144.
37 Matthews BW (1968) Solvent content of protein crystals. *J Mol Biol* **33**, 491–497.
38 McCoy AJ, Grosse-Kunstleve RW, Adams PD, Winn MD, Storoni LC and Read RJ (2007) Phaser crystallographic software. *J Appl Crystallogr* **40**, 658–674.
39 Emsley P and Cowtan K (2004) Coot: model-building tools for molecular graphics. *Acta Crystallogr D Biol Crystallogr* **60**, 2126–2132.
40 Emsley P, Lohkamp B, Scott WG and Cowtan K (2010) Features and development of Coot. *Acta Crystallogr D Biol Crystallogr* **66**, 486–501.
41 Murshudov GN, Skubak P, Lebedev AA, Pannu NS, Steiner RA, Nicholls RA, Winn MD, Long F and Vagin AA (2011) REFMAC5 for the refinement of macromolecular crystal structures. *Acta Crystallogr D Biol Crystallogr* **67**, 355–367.
42 Winn MD, Ballard CC, Cowtan KD, Dodson EJ, Emsley P, Evans PR, Keegan RM, Krissinel EB, Leslie AG, McCoy A *et al.* (2011) Overview of the CCP4 suite and current developments. *Acta Crystallogr D Biol Crystallogr* **67**, 235–242.
43 Liu FF, Kulinich A, Du YM, Liu L and Voglmeir J (2016) Sequential processing of mannose-containing glycans by two alpha-mannosidases from *Solitalea canadensis*. *Glycoconj J* **33**, 159–168.
44 Cheng K, Zhou Y and Neelamegham S (2016) DrawGlycan-SNFG: a robust tool to render glycans and glycopeptides with fragmentation information. *Glycobiology* **27**, 200–205.
45 Barsomian GD, Johnson TL, Borowski M, Denman J, Ollington JF, Hirani S, McNeilly DS and Rasmussen JR (1990) Cloning and expression of peptide-N4-(N-

acetyl-beta-D-glucosaminyl)asparagine amidase F in *Escherichia coli*. *J Biol Chem* **265**, 6967–6972.
46 Wang S, Wang PG and Qi Q (2007) Influence of substrate conformation on the deglycosylation of ribonuclease B by recombinant yeast peptide:N-glycanase. *Acta Biochim Biophys Sin* **39**, 8–14.
47 Morelle W and Michalski JC (2007) Analysis of protein glycosylation by mass spectrometry. *Nat Protoc* **2**, 1585–1602.
48 Doherty M, McManus CA, Duke R and Rudd PM (2012) High-throughput quantitative N-glycan analysis of glycoproteins. *Methods Mol Biol* **899**, 293–313.
49 Thompson AJ, Spears RJ, Zhu Y, Suits MDL, Williams SJ, Gilbert HJ and Davies GJ (2018) *Bacteroides thetaiotaomicron* generates diverse alpha-mannosidase activities through subtle evolution of a distal substrate-binding motif. *Acta Crystallogr D Struct Biol* **74**, 394–404.
50 Kurakata Y, Uechi A, Yoshida H, Kamitori S, Sakano Y, Nishikawa A and Tonozuka T (2008) Structural insights into the substrate specificity and function of *Escherichia coli* K12 YgjK, a glucosidase belonging to the glycoside hydrolase family 63. *J Mol Biol* **381**, 116–128.
51 Aleshin AE, Feng PH, Honzatko RB and Reilly PJ (2003) Crystal structure and evolution of a prokaryotic glucoamylase. *J Mol Biol* **327**, 61–73.
52 Hidaka M, Honda Y, Kitaoka M, Nirasawa S, Hayashi K, Wakagi T, Shoun H and Fushinobu S (2004) Chitobiose phosphorylase from *Vibrio proteolyticus*, a member of glycosyl transferase family 36, has a clan GH-L-like (alpha/alpha)(6) barrel fold. *Structure* **12**, 937–947.
53 Numao S, Kuntz DA, Withers SG and Rose DR (2003) Insights into the mechanism of *Drosophila melanogaster* Golgi alpha-mannosidase II through the structural analysis of covalent reaction intermediates. *J Biol Chem* **278**, 48074–48083.
54 Heikinheimo P, Helland R, leirosHK, Leiros I, Karisen S, Evjen G, Ravelli R, Schoehn G, Ruifrok R *et al.* (2003) The structure of bovine lysosomal alpha-mannosidase suggests a novel mechanism for low-pH activation. *J Mol Biol* **327**, 631–644.
55 Guerin DM, Lascombe MB, Costabel M, Souchon H, Lamzin V, Beguin P and Alzari PM (2002) Atomic (0.94 A) resolution structure of an inverting glycosidase in complex with substrate. *J Mol Biol* **316**, 1061–1069.
56 Attigani A, Sun L, Wang Q, Liu Y, Bai D, Li S and Huang X (2016) The crystal structure of the endoglucanase Cel10, a family 8 glycosyl hydrolase from *Klebsiella pneumoniae*. *Acta Crystallogr F Struct Biol Commun* **72**, 870–876.
57 Zheng H, Cooper DR, Porebski PJ, Shabalin IG, Handing KB and Minor W (2017) CheckMyMetal: a macromolecular metal-binding validation tool. *Acta Crystallogr D Struct Biol* **73**, 223–233.

Supporting information

Additional supporting information may be found online in the Supporting Information section at the end of the article.

Table S1. Data processing and refinement statistics for EfMan-I crystal structure.

Table S2. Protein sequence identities (%) among EfMan-I, SpGH92, Bt2199, and Bt3990.

Table S3. N-terminal sequencing results of the recombinant EfMan-I.

Fig. S1. Protein sequence alignment of EfMan-I (EF2217) with SpGH92, Bt2199, and Bt3990.

Fig. S2. Standard curve of para-nitrophenolate (pNP) (A) and GraFit graphs for determining the kinetics data of EfMan-I using ManαpNP as the substrate (B).

Fig. S3. Standard curve of mannose using coupled enzyme assays (A) and GraFit graphs for determining the kinetics data of EfMan-I using α2-mannobiose as the substrate (B).

Fig. S4. GraFit graphs for determining the kinetics data of EfMan-I using RNase B as the substrate.

Fig. S5. 1H NMR-based time course studies of EfMan-I-catalyzed hydrolysis of ManαpNP.

Fig. S6. MALDI-TOF analysis of high mannose N-linked glycans released from RNase B without (A) and with (B) EfMan-I treatment.

Fig. S7. MALDI-TOF analysis of 2-aminobenzamide (2-AB)-labeled high mannose N-linked glycans released from RNase B without (A) and with (B) EfMan-I treatment.

Graphical Abstract

The contents of this page will be used as part of the graphical abstract of html only. It will not be published as part of main article.

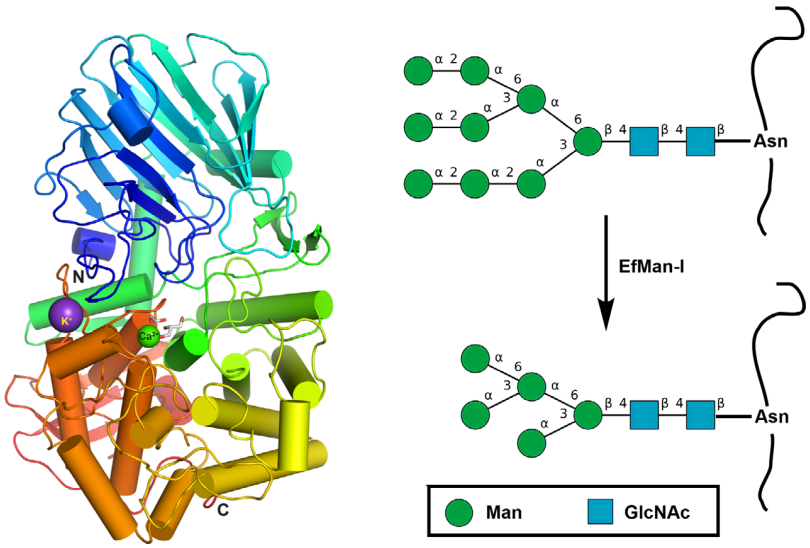

14 XXX.